Theoretical Equations of State for the Rare Gases

LOS ALAMOS SCIENTIFIC LABORATORY
Post Office Box 1663 Los Alamos, New Mexico 87545

This work was supported by the US Department of Energy, Office of Basic Energy Sciences.

LA-8062
UC-34
Issued: January 1980

Theoretical Equations of State for the Rare Gases

G. I. Kerley
P. M. Henry*

*LASL Graduate Research Assistant. Present address: Physics Department, University of Missouri, Columbia, MO 65201.

THEORETICAL EQUATIONS OF STATE FOR THE RARE GASES

by

G. I. Kerley and P. M. Henry

ABSTRACT

Theoretical equations of state and related calculations are reported for the rare gases neon, argon, krypton, and xenon. The liquid and vapor phases were computed using a model which is based upon thermodynamic perturbation theory. The fluid model requires an expression for the potential energy of a molecule in the force field of its neighbors; this function is derived from the zero-temperature isotherm of the solid. The solid isotherm was determined from static-compression data and statistical atom theory. The solid data were the only experimental information used to construct the liquid model. Comparisons are made with measured isothermal-compression data, sound speeds, vaporization curves, Hugoniots, structure factors, viscosities, and melting curves. Agreement with experiment is good.

I. INTRODUCTION

Argon and the other noble gases frequently are studied as test cases for theories of equations of state (EOS) and related material properties.[1,2] Many models assume that the intermolecular forces in these materials are pairwise additive; calculations have been made using pair potentials constructed from experimental data.[2] However, recent work has shown that intermolecular forces are not pairwise additive in rare gas solids and liquids.[2,3] The existence of three-body and higher order forces complicates the theory of these substances.

In this work, we apply the CRIS model to calculations for the rare gases. This model is an extension of previous work[4] on the theory of argon and hydrogen. The thermodynamic properties are computed from an expansion about a hard-sphere

fluid reference system, in which the hard sphere diameter is chosen by a variational principle. The theory differs from that of other investigators in the treatment of intermolecular forces and in the calculation of second- and higher-order terms in the expansion. The CRIS model uses the zero-temperature isotherm of the solid to define an expression for the energy of a molecule in the field of its neighbors. This approach avoids complications that arise when the intermolecular forces are explicitly separated into two-body, three-body, and other many-body potentials. In our previous work,[4] we carried the perturbation expansion to first order. In this report, we include contributions from higher-order terms in the expansion, using approximations derived from macroscopic fluctuation theory. Tests of the theory for the 6-12 and inverse power potentials showed that it agrees well with Monte Carlo and molecular dynamics calculations.[5]

The only information required to apply the liquid model is the zero-temperature isotherm of the solid. For this study, we constructed cold curves for the noble gases by fitting analytic expressions to static-compression data for the solid phases and used a formula related to statistical atom theory to extrapolate the data to higher densities. Sensitivity studies indicate that the cold curves for the noble gases are sufficiently accurate for this study, although new experimental and theoretical results to check our statistical atom predictions would be helpful.

The fluid model is described in Sec. II, and the solid model and cold curve calculations are described in Sec. III and Appendix A. In this study we applied the model to neon, argon, krypton, and xenon. We did not study helium because quantum effects, known to be important in that case, are not included in the model. In Sec. IV we compare our calculations with measured isothermal-compression data, sound speeds, vaporization data, Hugoniots, structure factors, viscosities, and melting curves. Agreement with experiment is very good. We also make theoretical predictions of the Hugoniots for liquid neon and krypton, which have not been measured.

In the Hugoniot calculations, we included contributions from thermal electronic excitation to the EOS. These terms were computed from statistical atom theory, as explained in Appendix B.

II. THE FLUID MODEL

In this section we describe the main features of the CRIS fluid model used in our calculations. A more detailed description of the theory will be published elsewhere.[5] Throughout this discussion, we assume that the molecules are in the ground electronic state. At high temperatures, these results must be corrected for electronic excitation of the atoms; these corrections are considered in Appendix B.

A. The Variational Method

Because the structure of liquids and dense gases is determined primarily by repulsive forces[2,6] (effects of excluded volume), it is useful to express the Helmholtz free energy as a perturbation expansion about a hard-sphere fluid.

$$A = A_o + \langle U \rangle_o + \Delta A \ , \tag{1}$$

where A_o is the free energy of the hard sphere system and U is the potential energy of the real system (a general function of the coordinates of the liquid molecules). The term $\langle U \rangle_o$ denotes an average of U taken in the hard-sphere system.

By definition, ΔA contains all remaining contributions to A; these corrections are due to differences between the structure of the real liquid and that of the hard-sphere system. This term can be made quite small by an appropriate choice of the hard-sphere diameter, σ_o. The first two terms in Eq. (1) give an upper bound to the free energy,[2]

$$\tilde{A} = A_o + \langle U \rangle_o \geq A \tag{2}$$

Our procedure is to minimize $\tilde{A}$ with respect to σ_o; in this way, we find the hard-sphere system whose structure is closest to that of the real fluid. Then the correction ΔA is small, and it is feasible to consider approximations to it (see Sec. C, below).

B. First-Order Theory

The function $\phi(\vec{q}_i)$ is the potential energy of the i-th molecule in the field of its neighbors. Here $\vec{q}_i$ are the coordinates of the neighbors relative to molecule i. In principle, ϕ can be expanded as a sum over pair, triplet, and higher-order interactions.

$$\phi(\vec{q}_i) = (1/2!)\Sigma_j\, u_2(ij) + (1/3!)\Sigma_{jk}\, u_3(ijk) + \cdots \quad . \tag{3}$$

For a particular configuration of the system, the total potential energy is a sum over all molecules.

$$U = \Sigma_i\, \phi(\vec{q}_i) \quad . \tag{4}$$

Each molecule has a different energy that depends upon the local arrangement of its neighbors. However, the <u>average</u> value of ϕ over all configurations of the system is the same for each molecule. Therefore, we can write

$$< U >_o = N < \phi >_o \tag{5}$$

and

$$< \phi >_o = \frac{1}{N} \int \cdots \int \phi(\vec{q})\, n_o(\vec{q})\, d\vec{q}_1\, d\vec{q}_2 \cdots \quad . \tag{6}$$

Here $n_o(\vec{q})$ is the average number density of molecules having a local arrangement $\vec{q}$ of its neighbors.

The function ϕ depends upon the short-range structure of the liquid, especially the number and positions of molecules in the first shell of neighbors. The CRIS model assumes that the nearest neighbors lie on a spherical shell. The nearest-neighbor distance R and the coordination number ν vary from molecule to molecule, but the volume per molecule is fixed at the mean macroscopic value V/N. Therefore, the coordination number is proportional to the volume of the first coordination sphere. By requiring a molecule to have 12 nearest neighbors in a close-packed configuration, we find that

$$\nu = 6\sqrt{2}\, NR^3/V \quad . \tag{7}$$

In this approximation only one variable, R, is required to specify the local arrangement of neighbors about a particular molecule. Equation (6) reduces to

$$< \phi >_o = \frac{1}{N} \int \phi(R,\nu)\, n_o(R)\, 4\pi R^2 dR \ , \tag{8}$$

where $n_o(R)$ is the number density of molecules having neighbors on a shell of radius R.

The distribution function $n_o(R)$ can be obtained from the radial distribution function (RDF) for hard spheres, $g_o(R)$. We find that

$$(N/V)\ g_o(R) = (\nu/N)\ n_o(R) \quad . \tag{9}$$

Here, and in subsequent equations, $g_o(R)$ refers to the first peak in the RDF, the contribution that corresponds to the nearest neighbors. To normalize $n_o(R)$ we introduce a cutoff in R, as follows.

$$\int_o^{R_M} n_o(R)\ 4\pi R^2 dR = N \quad . \tag{10}$$

The potential-energy function $\phi(R,\nu)$ can be estimated from the zero-temperature isotherm of the solid in the following way. Let $E_c(V)$ be the electronic contribution to the energy per molecule for the close-packed solid at volume V and zero temperature. (Here, and in subsequent equations, contributions from zero-point motion of the nuclei are not included in the definition of E_c.) The volume V is related to the nearest-neighbor distance by

$$V = NR^3/\sqrt{2} \quad . \tag{11}$$

In the liquid phase, a molecule has the same potential energy as it would in the solid phase at the same nearest-neighbor distance, except that the number of neighbors has been reduced from 12 to ν. Hence,

$$\phi(R,\nu) = (\nu/12)\ E_c(NR^3/\sqrt{2}) \quad . \tag{12}$$

Using the above expressions we find

$$< \phi >_o = \frac{\pi N}{3V} \int_o^{R_M} E_C(NR^3/\sqrt{2})\ g_o(R)\ R^2 dR \quad . \tag{13}$$

We use Eq. (13) and the free-energy and RDF formulas for the hard-sphere reference system[5] to define our first-order estimate of the Helmholtz free energy, $\tilde{A}$. We minimize $\tilde{A}$ to obtain the hard-sphere diameter as a function of density and temperature. The first-order approximations to the internal energy and pressure are computed from standard thermodynamic relationships. It is found that[4]

$$\tilde{E} = \frac{3}{2} NkT + N < \phi >_o \tag{14}$$

and

$$\tilde{P} = \frac{NkT}{V} + \frac{\pi N^2}{3V} \int_o^{R_M} P_C(NR^3/\sqrt{2})\ g_o(R)\ R^2 dR \quad , \tag{15}$$

where $P_C(V)$ is the pressure on the zero-temperature isotherm of the solid.

C. Corrections to First-Order Theory

When the first-order theory is used in actual computation, the higher-order terms in the expansion are small but not negligible. For the inverse-12 potential, ΔA accounts for 5-10% of the free energy. The new approximations derived for these corrections yielded excellent results when the theory was compared with machine-calculated test cases.[5]

The potential energy for a perturbed fluid is

$$U_C(\lambda) = U_o + \lambda U \quad , \tag{16}$$

where U_o is the hard-sphere potential energy. Using standard λ-expansion techniques[6], we find the free energy of this perturbed system to be

$$A_C(1) = \tilde{A} + \int \cdots \int d\vec{q}_1 d\vec{q}_2 \cdots [\phi(\vec{q}) - < \phi >_o] \int_o^1 n_\lambda(\vec{q}) d\lambda \ , \tag{17}$$

where $n_\lambda(\vec{q})$ is the distribution function for the perturbed system and the other quantities are defined above. Note that $A_C \to \tilde{A}$ as $n_\lambda \to n_o$.

The perturbation redistributes the number of particles in configuration space from $n_o(\vec{q})$ to $n_\lambda(\vec{q})$. For a particular configuration $\vec{q}$, the change in the number of molecules is related to a fluctuation in the total number of molecules in the system. We can write an exact relation

$$n_\lambda(\vec{q}) = n_o(\vec{q};\mu) \ , \tag{18}$$

where μ is a perturbed chemical potential. The total number of particles associated with μ is $N(\mu)$, where

$$\mu \, N(\mu) = A_o(V,T,\mu) + V \, P_o(V,T,\mu) \ . \tag{19}$$

Our approximation is based upon the following expression for the perturbed chemical potential.

$$\mu(\vec{q},\lambda) \cong \mu_o - \lambda \, [\phi(\vec{q}) - \langle \phi \rangle_o] \ , \tag{20}$$

where μ_o is the chemical potential for the hard-sphere system at the macroscopic density. Hence, μ is related to the instantaneous fluctuation in the potential energy of a molecule about its mean value. The details of our argument are given in Ref. 5.

We apply this result to the liquid structure model described above to obtain the following result for the RDF of the perturbed system.

$$g_\lambda(R) \cong \frac{V}{N^2} \, \nu(\mu) \, n_o(R;\mu) \cong \left[\frac{N(\mu)}{N}\right]^2 g_o(R;\mu) \ , \tag{21}$$

where $N \equiv N(\mu_o)$. Hence the RDF of the perturbed system is related to that of the hard-sphere system undergoing a density fluctuation. Equation (21) gives good results when applied to test cases, in support of the approximation.

We can also apply the arguments given for the first-order theory to Eq. (17) to obtain

$$A_C(1) - \tilde{A} \cong N \frac{\sqrt{2}\pi}{3} \int_0^{R_M} \frac{dR}{R} \int_{\mu_o}^{\mu(1)} \left[\frac{N(\mu)}{N}\right]^2 g_o(R;\mu)d\mu \ . \tag{22}$$

The quantity $A_C(1)$ is the free energy of the real system plus a hard core; the integral over R in Eq. (22) makes no contribution for $R > \sigma_o$. To complete the derivation of ΔA, we add a second term to Eq. (22). A second perturbed potential energy is defined by

$$U_W(\lambda) = U + \lambda W_o \ , \tag{23}$$

$$W_o = \Sigma_{i>j} \ w_o(|\vec{R}_i - \vec{R}_j|), \tag{24}$$

and

$$w_o(R) = \begin{cases} \varepsilon & R > \sigma_o \\ o & R < \sigma_o \end{cases} \ ,$$

where ε is a constant having dimensions of energy. In the limit $\varepsilon \to \infty$, $W_o \to U_o$. Denote the free energy of this system by $A_W(\lambda)$. The λ-expansion can be used to give

$$A_W(\lambda \to \infty) = A_C(1) = A + N \ 2\pi\frac{N}{V} \ \varepsilon \int_0^{\sigma_o} R^2 dR \int_0^{\infty} g_W(R,\lambda)d\lambda \ , \tag{25}$$

where g_W is the RDF of the perturbed system. The blip function theory of Andersen et al.[7] suggests the following approximation for g_W.

$$g_W(R,\lambda) \cong \exp[-\beta\lambda w_o(R)]g(R) \ . \tag{26}$$

Using this result we obtain

$$A_C(1) \cong A + NkT \ 2\pi \frac{N}{V} \int_0^{\sigma_o} g(R)R^2 dR \ . \tag{27}$$

For g(R), we use Eq. (21) and extrapolate $g_o(R)$ inside the hard core.

Finally, we eliminate the quantity $A_C(1)$ from Eqs. (22) and (27), giving

$$\Delta A = A - \tilde{A} \cong -NkT\ 2\pi \frac{N}{V} \int_o^{\sigma_o} g(R)R^2 dR$$

$$+ N \frac{\sqrt{2}\pi}{3} \int_o^{R_M} \frac{dR}{R} \int_{\mu_o}^{\mu(1)} \left[\frac{N(\mu)}{N}\right]^2 g_o(R;\mu)\ d\mu \quad . \tag{28}$$

Further examination of the approximations used to derive Eq. (28) indicates that this result should be most accurate when σ_o is chosen by the variational principle. Therefore, we use the first-order theory to compute σ_o, $\tilde{A}$, $\tilde{E}$, and $\tilde{P}$ as functions of density and temperature. Equation (28) is used to compute the higher-order corrections to A. Energy and pressure corrections are calculated by numerical differentiation of Eq. (28), using the standard thermodynamic expressions.

III. THE SOLID MODEL

For this study, we constructed the zero-temperature isotherms required for the CRIS model by fitting the Debye model to low-temperature compression data for the solids. We used a formula based on statistical atom theory to extend the results to higher densities, where no experimental data exist. Trickey and Green[8] have obtained good results by applying band-theoretical methods to the rare gases. Similar calculations, to check our cold curve at high densities, are being made at this laboratory.

A. Low-Density Formula

For pressures less than about 10 GPa, we used the following formulas for the cold curve.

$$E_C(\rho) = a_1 \exp(-a_2/\rho^{1/3}) - a_3\rho^2 \tag{29}$$

and

$$P_C(\rho) = (1/3)a_1a_2\rho^{2/3}\exp(-a_2/\rho^{1/3}) - 2\ a_3\ \rho^3 \quad . \tag{30}$$

One relation among a_1, a_2, and a_3 was obtained from the binding energy of the solid; Eq. (30) was fit to the compression data subject to this constraint, with zero-point and thermal corrections computed as described below. Fit parameters for the four gases are given in Table I. Units are chosen so that E_c is in MJ/kg, P_c is in GPa, and ρ is in Mg/m^3.

Equations (29) and (30) are closely related to the Buckingham (exp-6) potential, which is frequently used for the noble gases.[9,10]

$$u_2(R) = \frac{\varepsilon}{\alpha-6}\left[6\, e^{\alpha(1-R/\sigma)} - \alpha\left(\frac{\sigma}{R}\right)^6\right] \quad . \tag{31}$$

The cold curve can be computed in the usual way by summing Eq. (31) over all pairs of molecules. If only nearest neighbors are considered in the exponential term, the result agrees with Eq. (29). Equation (31) is not used explicitly in any of our fluid calculations, and we do not propose this form as the best potential for the rare gases. However, the coefficients of our fit are in reasonable agreement with the potential parameters ε, α, and σ that have been proposed by others.[9,10]

B. High-Density Formula

The exp-6 formula can be used for all of our liquid calculations except the Hugoniots. Because the shock-wave data go to much higher densities than were studied in the solid experiments, we had to use a different expression for the cold curve in this region. Our high-density equation, discussed in Appendix A, is an interpolation formula joined continuously and smoothly to the low-density expression. It reduces to the Thomas-Fermi-Dirac (TFD) theory at high densities. The two expressions were matched at about 10 GPa (the upper limit of the xenon data) in all four cases. The TFD-match density (ρ_M) for each of the four gases is given in Table I.

In the absence of other data, our method for defining the cold curve at high densities seems to be reasonable. The TFD and exp-6 formulas agree up to about 40 GPa, well beyond the point at which they are joined. The Hugoniot calculations are the only results affected by the high-density portion of the curve. For solid argon, changing the TFD-match density by ±20% causes a ±2% change in the shock velocity at the highest pressure studied; the value chosen gives the best agreement with experiment. Hence, the uncertainty in our shock-wave predictions is small, if not negligible.

C. Debye Model

For comparison with experimental solid data, contributions from zero-point and thermal lattice vibrations must be added to Eqs. (29) and (30). We used the Debye model, which assumes the following expressions.[11]

$$A(\rho,T) = E_C(\rho) + \frac{9}{8} Nk\Theta + NkT[3\ln(1 - e^{-\Theta/T}) - D(\Theta/T)] \quad , \tag{32}$$

$$E(\rho,T) = E_C(\rho) + \frac{9}{8} Nk\Theta + 3NkT\, D(\Theta/T) \quad , \tag{33}$$

$$P(\rho,T) = P_C(\rho) + \gamma\rho \left[\frac{9}{8} Nk\Theta + 3NkT\, D(\Theta/T)\right] \quad , \tag{34}$$

and

$$D(\Theta/T) = \frac{3T^3}{\Theta^3} \int_0^{\Theta/T} \frac{y^3 dy}{e^y - 1} \quad , \tag{35}$$

where Θ is the Debye temperature and γ is the Grüneisen function, defined by

$$\gamma = d(\ln \Theta)/d(\ln \rho) \quad . \tag{36}$$

Both Θ and γ are taken to be independent of temperature. The density dependencies were assumed to have the forms

$$\gamma = \gamma_o(\rho_o/\rho) + (2/3)(1 - \rho_o/\rho) \tag{37}$$

and

$$\Theta = \Theta_o \exp\left[\int_{\rho_o}^{\rho} \frac{\gamma(x)}{x}\, dx\right] \quad , \tag{38}$$

where ρ_o, Θ_o, and γ_o were taken from experiment[12] and are given in Table I. The Grüneisen function γ varies by about 10-25% over the density range of the experimental data, and the lattice vibration corrections are relatively small at the

TABLE I

COLD CURVE AND SOLID MODEL PARAMETERS

Parameter	Neon	Argon	Krypton	Xenon
a_1	2.7314×10^5	3.2215×10^5	1.1589×10^5	5.0308×10^4
a_2	17.815	17.888	20.34	20.45
a_3	0.074860	0.10646	0.025142	0.015670
ρ_M	3.0	2.9	5.0	6.0
ρ_o	1.4666	1.6509	3.0786	3.7461
$\theta_o^o(K)$[a]	67.	95.	64.5	49.
γ_o	2.68	2.61	2.05	2.91

[a]From Ref. 12.

high densities. Consequently, Eqs. (37) and (38) are sufficiently accurate for our purposes.

Figure 1 shows the Helmholtz free energy versus temperatures for the rare gas solids. Agreement between the Debye model and the experimental data[13] is not satisfactory at high temperatures. The results are particularly poor for argon, which has large anharmonic effects.[14] At low temperatures, the theory is adequate for computing the small lattice corrections to the cold curve. However, the solid model is too poor to give meaningful results in the study of melting. Figure 1 shows that the Debye model gives best results for krypton; our calculation of the melting curve for krypton is given in Sec. IV. Better theories of the rare-gas solids exist[1], but were not considered in this work.

Low temperature isotherms for the rare gas solids are displayed in Figs. 2-5. The EOS of solid neon, argon, and krypton have been measured to 2 GPa[15,16] at 4.2 K. For argon, two high-pressure points have been reported by Homan et al.[17] Xenon has been measured to 11 GPa at 85 K.[18] Our calculated curves agree with the experimental data at low pressures and with the TFD data at high pressures.

IV. CALCULATIONS AND RESULTS

Comparisons of the fluid model with isothermal compression data, sound speeds, vaporization curves, Hugoniots, structure factors, viscosities, and melting curves show good agreement. All computations were done using the PANDA code, a multipurpose EOS program.

A. Isothermal Compression Data

EOS for the four rare-gas liquids are shown in Figs. 6-9. Isotherms for the solid phases are included for comparison. Experimental data were taken from Refs. 15-26.

The most extensive PVT data are available for argon, which is typical of the results obtained in all four cases. Figure 7 shows that the CRIS model accurately predicts the expansion that occurs at melting and upon heating of the liquid. The density dependence of the pressure along a given isotherm is in good agreement for all of the rare gases.

In Fig. 10 we compare our calculated sound speeds as a function of pressure with experimental data from Ref. 20. The pressure dependence and the trends among the four rare gases are in good agreement with the measurements.

As stated above, the calculated liquid properties depend only on the exp-6 formulas for the cold curve, which we obtained by fitting the solid data. The results are not affected by changes to the high-density (TFD) portions of the cold curves.

B. Vaporization Data

At low temperatures, isotherms calculated using the CRIS model display Van der Waals loops, indicating the existence of a vapor-liquid coexistence region and a critical point. The EOS surface for argon in the critical point region is shown in Fig. 11. Above 160 K, only one phase is stable. At temperatures below the critical point, vaporization occurs at the pressure where the two phases have equal Gibbs free energies. In Figs. 12-18, we compare our calculated vaporization properties with experimental data from Ref. 27.

Vapor-pressure curves for the rare-gas liquids (Fig. 12) show that there is good agreement between the calculations and the experimental data. The model accurately predicts the temperature dependence of the pressure and the trends among the elements.

Densities of the saturated vapor and saturated liquid are shown for the rare gases in Figs. 13-16. Agreement is good, especially for argon and krypton.

Calculated and experimental critical parameters for the rare gases are compared in Table II. Figures 13-16 and Table II show show that our calculated critical temperatures are too high by 6-10%. This discrepancy indicates that the long-range fluctuations known to be important near the critical point are not adequately described by our approximation to the high-order terms in the perturbation expansion. Our results for argon agree with the calculations of Barker et al.,[3] who included 3-body interactions.

Entropy on the coexistence curve is shown for neon in Fig. 17 and for argon in Fig. 18. Theoretical densities for the saturated liquid and vapor were used in the calculations (shown by a solid line). Agreement with the data is fairly good, but there are some discrepancies. Most of the disagreement arises from use of the theoretical densities. The dashed curve shows calculations using the experimental liquid and vapor densities; in this case, agreement with the experimental entropy data is very good.

Our calculated vaporization properties are in poorest agreement with experimental data for neon. Part of the discrepancy is due to quantum effects that are not taken into account in our model. Singh and Sinha[28] have computed quantum corrections to the hard-sphere fluid as a power series in λ/σ_o, where λ is the thermal wavelength,

$$\lambda = (h^2/2\pi WkT)^{\frac{1}{2}} \quad , \tag{39}$$

and σ_o is the hard-sphere diameter. For liquid neon at 25 K, λ = 0.777 Å. The CRIS model predicts σ_o = 2.82 Å and $N\sigma_o^3/V$ = 0.826. The quantum corection to the pressure is about 6.5 MPa, which corresponds to a 2% shift in the liquid density. Hence, the effect is small, but not negligible. A complete theory for calculating quantum corrections does not exist at this time.

TABLE II

CRITICAL PARAMETERS FOR THE RARE GASES

Parameter		Neon	Argon	Krypton	Xenon
T_C(K)	calc	47.2	159.	225.	318.
	exp[a]	44.4	151.	209.	290.
P_C(MPa)	calc	3.18	5.94	6.90	7.66
	exp[a]	2.65	5.00	5.49	5.83
ρ_c(Mg/m^3)	calc	0.431	0.503	0.795	0.968
	exp[a]	0.483	0.536	0.911	1.11

[a]From Ref. 27.

C. Shock Hugoniot Data

Shock-wave measurements provide a good test for our liquid model at high densities. We have calculated Hugoniots for all four rare gases using the standard relation

$$E_H - E_o = \tfrac{1}{2} (P_H + P_o) (\rho_o^{-1} - \rho_H^{-1}) \quad , \tag{40}$$

where E_H, P_H, and ρ_H are the Hugoniot energy, pressure, and density, respectively, and E_o, P_o, and ρ_o are the initial conditions. The particle velocity U_P and shock velocity U_S are related to the pressure and density by

$$U_P = (P_H - P_o)(\rho_o^{-1} - \rho_H^{-1}) \tag{41}$$

and

$$U_S = U_P/(1 - \rho_o/\rho_H) \quad . \tag{42}$$

The Hugoniot experiments considered here reach temperatures that are high enough ($> 10^4$ K) to cause significant amounts of electronic excitation in atoms. For this study we used the temperature dependent-TFD theory to compute contributions to the EOS from thermal electronic excitation.[29] The calculations are discussed in Appendix B.

Several shock-wave experiments have been performed on argon. Figure 19 shows the Hugoniot[30] for an initial temperature of 75 K. Although initially in the solid state, argon melts when shocked to sufficiently high pressures, and most of the data lie in the liquid region. The solid line is our calculation for the liquid, which includes corrections for electronic excitation. Agreement with the high-pressure data is good. The dashed curve is a calculation which does not include the electronic terms; the effect is small, but significant. The dashed-dotted line is a calculation for the shocked solid; agreement with the low-pressure data is fairly good.

Hugoniots for liquid argon at two different initial temperatures[31] are shown in Fig. 20. Agreement is very good when the electronic terms are included in the calculation. These corrections are particularly important for the 148 K initial state.

The Hugoniot[32] for argon shocked from an initial temperature of 300 K is displayed in Fig. 21. In these experiments the initial density is low (.0013 Mg/m^3), and there is enough thermal energy to cause large amounts of electronic excitation. Figure 21 shows that agreement with the data is very poor unless the electronic terms are included in the calculation. This drastic case shows that our TFD model used to compute the electronic corrections gives reasonable results.

Results[33] for doubly shocked argon are shown in Fig. 22. These experiments are especially interesting because the second (reflected) shock state reaches a high density without as much thermal heating as in the other experiments. Hence, the measurements provide a good test of the cold curve and the liquid model at high densities. Agreement between our calculations and the data is very good.

The Hugoniot[34] for xenon is shown in Fig. 23. Xenon has attracted interest because the two high-pressure experiments gave considerably lower shock velocities than would be expected from simple extrapolations of the low-pressure data;[35] there may be a transition to a metallic state.[36] Our calculations for xenon are better than those for the other rare gases because the solid data used to construct the cold curve go to much higher pressures. Figure 23 shows that our results are in fairly good agreement with the data. The effects of electronic excitation are significant because they account for a large part of the "softness" at high pressures. Additional shock-wave and static data for xenon would be welcome.

We also predicted the Hugoniots for neon and krypton, which have not been measured. The triple points were chosen as the initial states in both cases. The calculated Hugoniots are given in Figs. 24 and 25. Experiments on these two materials would provide a test of the predictive power of our theory.

D. Radial Distribution Function and Structure Factor

The CRIS model can be used to calculate the first peak in the RDF, as described in Sec. II, Eq. (21). The structure factor is defined by

$$S(K) = 1 + \frac{N}{V} \int [g(R) - 1] e^{i\vec{K}\cdot\vec{R}} \, d\vec{R} \quad . \tag{43}$$

It is convenient to write S(K) as the sum of two terms.

$$S(K) = S_o(K) + \Delta S(K) \tag{44}$$

and

$$\Delta S(K) = \frac{N}{V} \int [g(R) - g_o(R)] e^{i\vec{K}\cdot\vec{R}} \, d\vec{R} \quad . \tag{45}$$

We computed $S_o(K)$, the hard-sphere structure factor, from the equations of Verlet and Weis[37] and our hard-sphere diameter as predicted by the CRIS model. The terms $g(R)$ and $g_o(R)$ differ primarily in the nearest-neighbor peak, where $g_o(R)$ has a sharp cutoff at the hard-sphere diameter. The quantity $\Delta S(K)$ is found to be fairly small because it is spread out over all values of K. In this report we calculate $\Delta S(K)$ from our expression for $g(R)$, including only the first peak.

In Fig. 26 we compare our calculated structure factor for neon with measurements obtained by neutron diffraction.[38] The hard-sphere result, $S_o(K)$, is shown by a dashed line; the solid line includes the soft-core correction, $\Delta S(K)$. Differences between the two calculations are small, as explained above. Agreement with experiment is good.

The calculated and measured radial distribution functions[39] for argon at 85 K are compared in Fig. 27. Only the first peak is calculated by the theory. Agreement is good, although the calculated peak lies slightly to the left of the measured peak. Comparisons between the theoretical and experimental peak heights and peak positions[39,40] for three cases are given in Table III.

TABLE III

CALCULATED AND EXPERIMENTAL PEAK HEIGHTS AND POSITIONS

FOR RADIAL DISTRIBUTION FUNCTIONS OF LIQUID ARGON

Density (Mg/m^3)	Temperature (K)	Peak Height		Peak Position (Å)	
		Calc	Exp	Calc	Exp
1.409	85.	3.13	3.05	3.56	3.68
1.116	127.	2.17	2.11	3.65	3.83
.91	143.	2.08	2.02	3.72	3.82

[a] From Refs. 39 & 40.

E. Viscosity

Dymond and Alder[41] proposed a hard-sphere model for calculating transport coefficients in simple liquids. They asserted that repulsive forces play the dominant role in transport phenomena. To a rough approximation, the molecules are in free flight between collisions when they are in the attractive regions of the potential. Deviations from this simple picture can be calculated by perturbation theory,[42] but the corrections are presumed to be small.

We found that the hard-sphere approximation gives good results for the viscosities of the noble gases. We used the CRIS model to define the hard-sphere diameter as a function of density and temperature. The shear viscosity is calculated from Dymond's fit[43] to the molecular dynamics results.[44]

$$V_S = \frac{5}{16\ \sigma_o^2} \left(\frac{WkT}{\pi}\right)^{\frac{1}{2}} \frac{6.1525\ \eta}{1 - 1.869\ \eta} \quad , \tag{46}$$

where $\eta = \pi N \sigma_o^3 / 6V$ is the packing fraction. The bulk viscosity is not as well known, but the molecular-dynamics calculations suggest that the Enskog result should be a fairly good approximation for this quantity.[44] Hence, we compute the bulk viscosity from the equation

$$V_B = \frac{16}{\pi \sigma_o^2} \left(\frac{WkT}{\pi}\right)^{\frac{1}{2}} \eta^2\ g_o(\sigma_o) \quad , \tag{47}$$

where $g_o(\sigma_o)$ is the hard-sphere RDF at contact.

In Fig. 28 we compare our computations with measured shear viscosities for liquid argon, krypton, and xenon.[45] The solid lines show calculations that used the theoretical liquid densities on the coexistence curve. The dashed lines show calculations which used the experimental liquid densities. The hard-sphere model successfully predicts the magnitude, temperature dependence, and trend among the three elements. Agreement with the data is better than 25%. These results are encouraging; better agreement should be obtained if corrections to the simple model are computed.

Additional comparisons of the calculated and experimental bulk and shear viscosities are shown in Table IV. The model does not do as well for bulk viscosity as it does for shear — the magnitude is roughly correct, but the temperature dependence is wrong. Part of the discrepancy may be due to our use of the

TABLE IV

SHEAR AND BULK VISOCITIES FOR LIQUID ARGON, KRYPTON, AND XENON

	Density (Mg/m^3)	Temperature (K)	Shear Viscosity ($10^{-3}P$) Calc	Shear Viscosity ($10^{-3}P$) Exp[a]	Bulk Viscosity ($10^{-3}P$) Calc	Bulk Viscosity ($10^{-3}P$) Exp[a]
	1.40	85.68	2.05	2.67	1.85	1.20
Argon	1.32	97.92	1.55	1.82	1.49	1.80
	1.24	109.60	1.24	1.31	1.20	2.30
	2.44	117.12	3.33	4.32	2.94	2.05
Krypton	2.38	125.26	2.89	3.65	2.68	2.62
	2.33	131.13	2.61	3.30	2.47	3.00
	2.93	168.63	3.62	4.77	3.34	1.7
Xenon	2.46	229.12	1.92	2.04	1.83	1.7
	1.96	270.54	1.15	1.21	0.91	3.5

[a]From Ref. 45.

Enskog formula, Eq. (47). Molecular-dynamics calculations show that deviations from Eq. (47) may be as large as 40% and that they depend upon the packing fraction.[44] However, existing numerical results are not accurate enough to justify use of a corrected formula for the bulk viscosity.

F. Melting Curve

In principle, melting curves for the rare gases can be computed from our theoretical models of the solid and liquid phases. The melting line is the pressure-temperature locus at which the two phases have equal Gibbs free energies. Because the melting curve depends upon free energy differences, it is very sensitive to small errors and provides an important test of the solid and liquid models.

In this study we found that the Debye model constructed for the solids was not good enough for use in computing melting curves. As shown in Fig. 1, it applies best to krypton. Our calculated melting curve for krypton (Fig. 29) shows fair agreement with the experimental data.[46] This result preliminary; we need a better solid model for the study of melting.

Although we do not show the results, the calculated melting curve for neon showed discrepancies that may be caused by neglecting quantum effects in the

liquid model, as discussed above. We plan to study the problem of quantum corrections in future work on melting curves for neon.

V. CONCLUSIONS

The CRIS fluid model gives a very good description of the properties of rare-gas liquids. To apply the theory, we must compute the zero-temperature isotherm of the solid, which describes the potential energy of a molecule in the field of its neighbors. In this study, we obtained the solid isotherm by fitting an analytic formula to experimental compression data, corrected for zero-point and thermal lattice contributions. The liquid model accurately predicts the EOS, sound speeds, vapor pressures and coexistence properties, and distribution functions for the rare-gas liquids. A hard-sphere model gave good results for the shear viscosity.

To calculate the shock-wave properties, we extended the cold curves to higher densities using a formula based upon statistical atom theory. Corrections for thermal electronic excitation were computed from statistical atom theory. The theory gave good agreement with measured shock data for argon and xenon, and predictions were made for the Hugoniots of neon and krypton.

There are several problems that deserve further study. Band-theoretical calculations and static-compression measurements would be useful to check our predictions for the cold curve at high densities. Quantum corrections to the properties of neon should be investigated. A better model of the rare gas solids must be developed for use in studying melting properties. Finally, further studies of transport properties, especially the bulk viscosity, would be helpful.

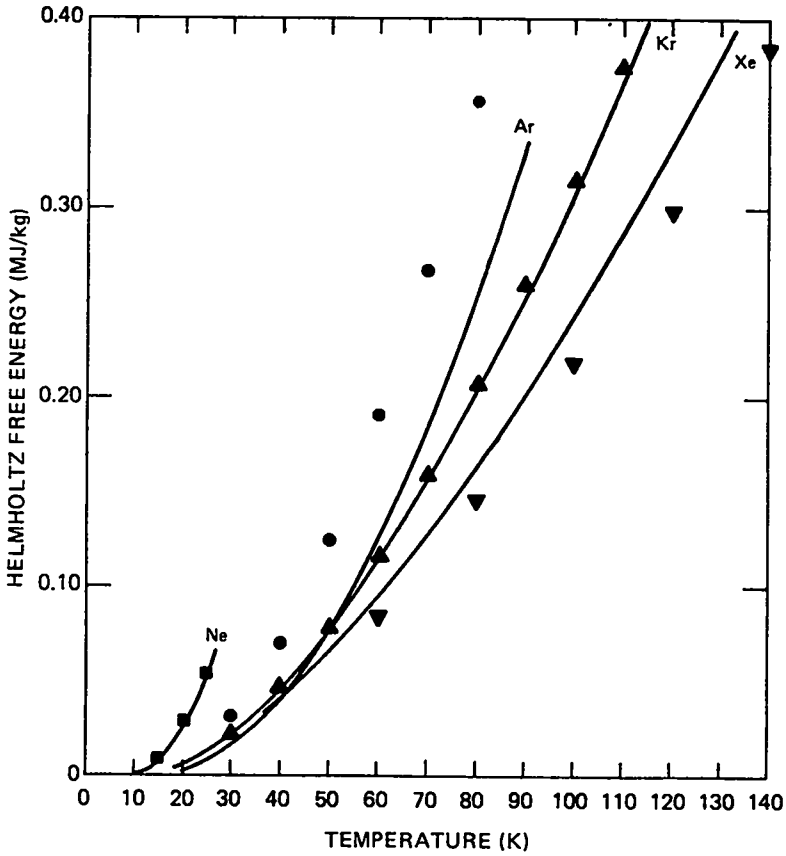

Fig. 1.
Helmholtz free energy vs temperature for the solid rare gases at zero pressure. Experimental data are from Ref. 13. The solid lines were calculated from the Debye model.

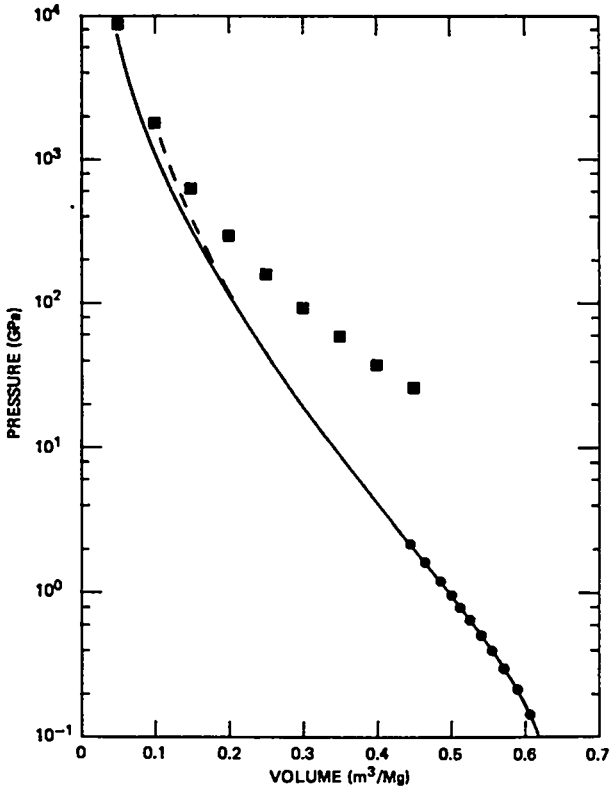

Fig. 2.
EOS for solid neon at 4.2 K. Circles are experimental data from Ref. 15 and squares are values computed using TFD theory. The solid line was calculated from the solid model used in this study. For comparison, the dashed line shows an extrapolation of the low-density formula for the cold curve to high densities.

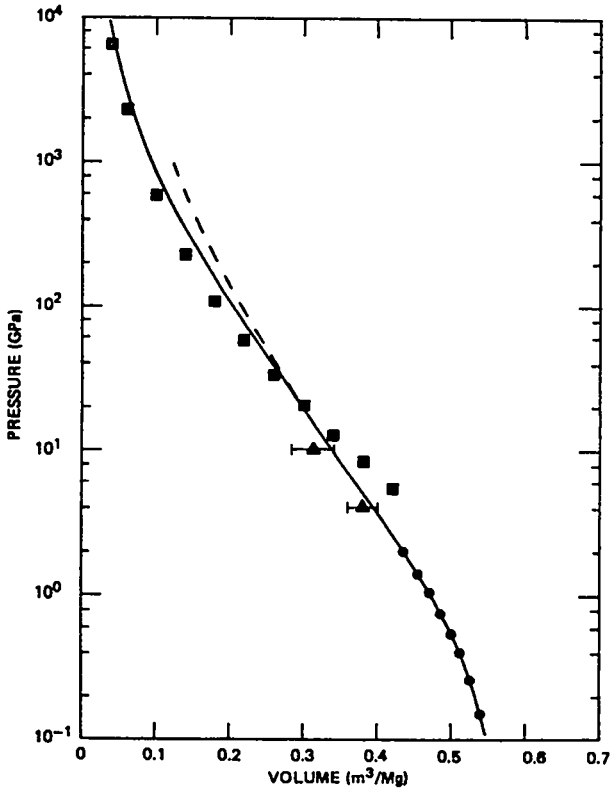

Fig. 3.
EOS for solid argon at 4.2 K. Circles are experimental data from Ref. 16 and triangles are data from Ref. 17. Other symbols are the same as in Fig. 2.

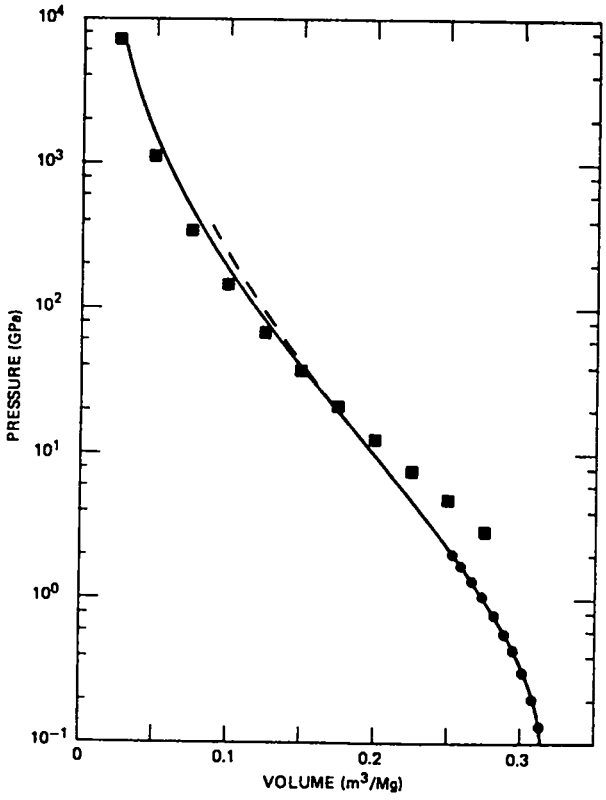

Fig. 4.
EOS for solid krypton at 4.2 K. Circles are experimental data from Ref. 16. Other symbols are the same as in Fig. 2.

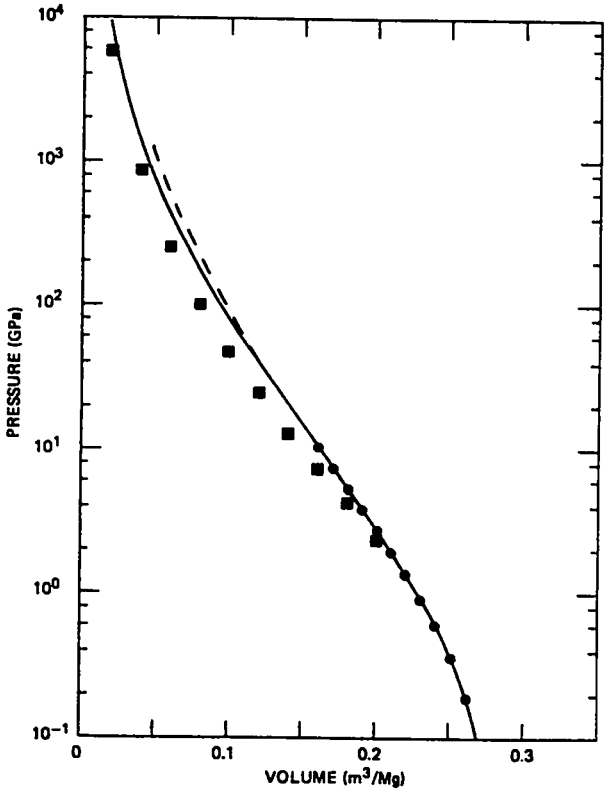

Fig. 5.
EOS for solid xenon at 85 K. Circles are experimental data from Ref. 18. Other symbols are the same as in Fig. 2.

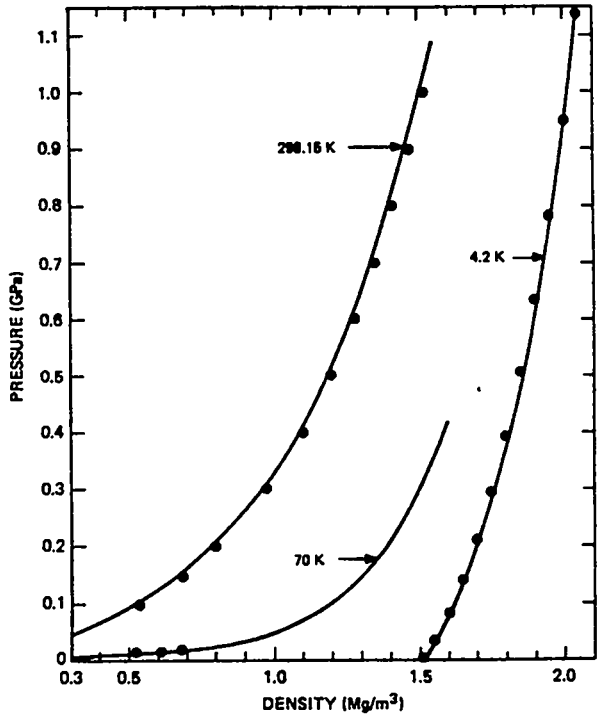

Fig. 6.
EOS for solid and liquid neon. Data for solid neon at 4.2 K are from Ref. 15. Data for liquid neon are from Refs. 19 and 20. The solid lines are our calculations.

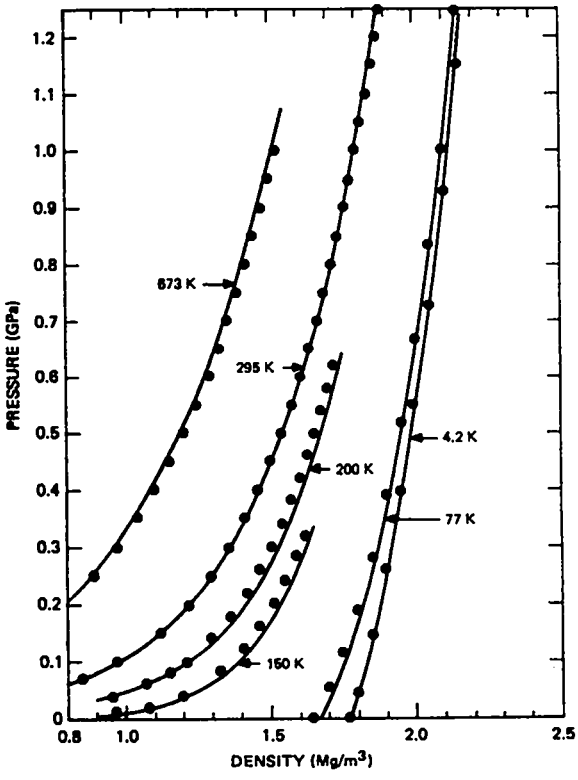

Fig. 7.
EOS for solid and liquid argon. Data for solid argon at 4.2 and 77 K are from Ref. 16. Data for liquid argon are from Refs. 21-24. The solid lines are our calculations.

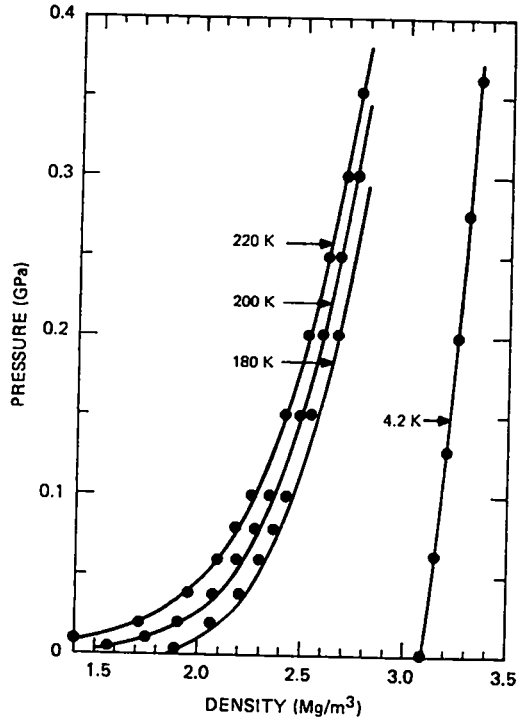

Fig. 8.
EOS for solid and liquid krypton. Data for solid krypton at 4.2 K from Ref. 16. Data for liquid krypton are from Ref. 25. The solid lines are our calculations.

Fig. 9.
EOS for solid and liquid xenon. Data for solid xenon at 85 K are from Ref. 18. Data for liquid xenon are from Ref. 26. The solid lines are our calculations.

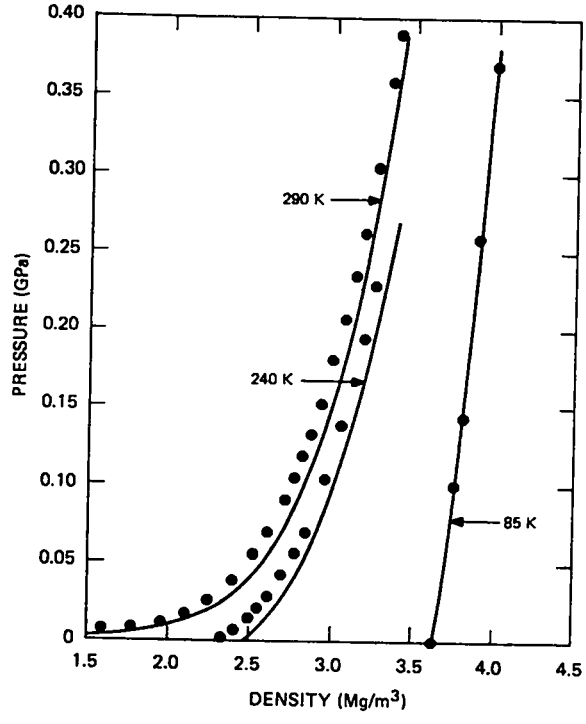

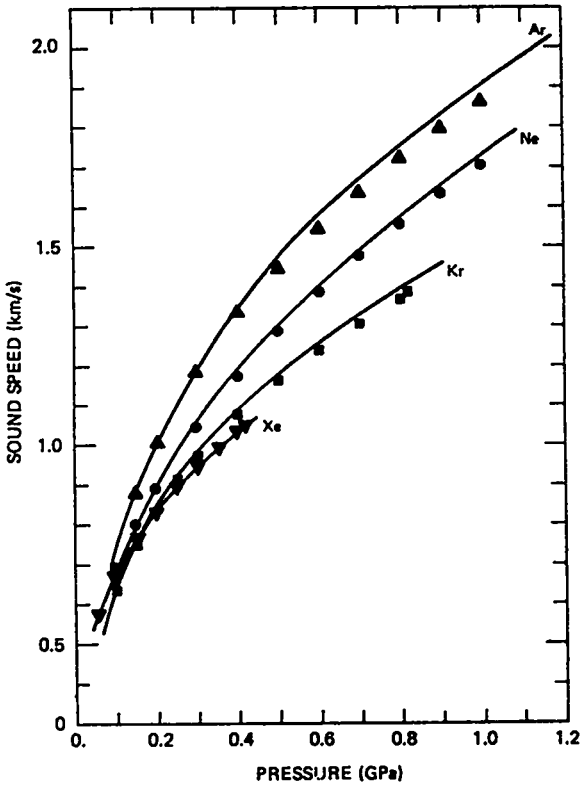

Fig. 10.
Sound speeds for the rare gases at 298.15 K. The solid lines are our calculations. Experimental data are from Ref. 20.

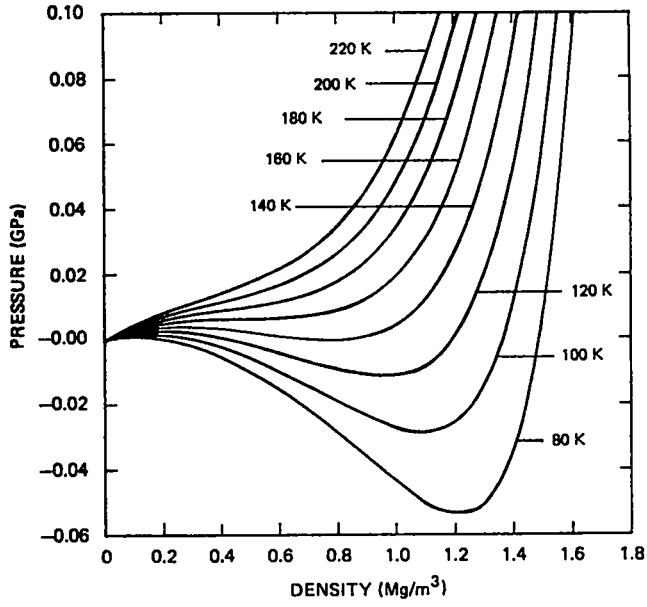

Fig. 11.
Calculated EOS for argon in the critical point region.

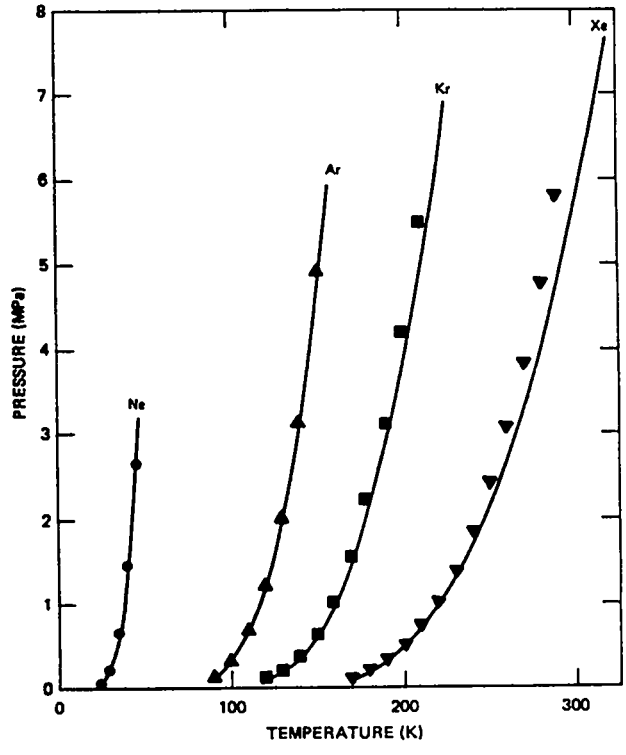

Fig. 12.
Vapor pressures for the rare-gas liquids. The solid lines are our calculations. Experimental data are from Ref. 27.

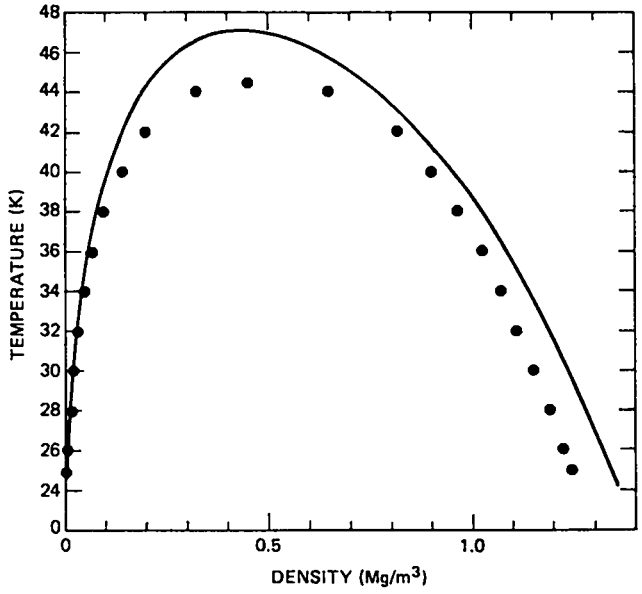

Fig. 13.
Temperature and density on the coexistence curve for neon. The solid line is our calculations. Experimental data are from Ref. 27.

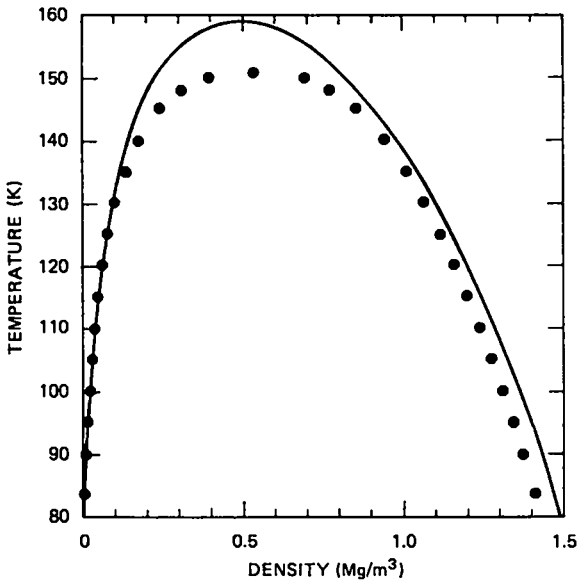

Fig. 14.
Temperature and density on the coexistence curve for argon. Symbols are the same as in Fig. 13.

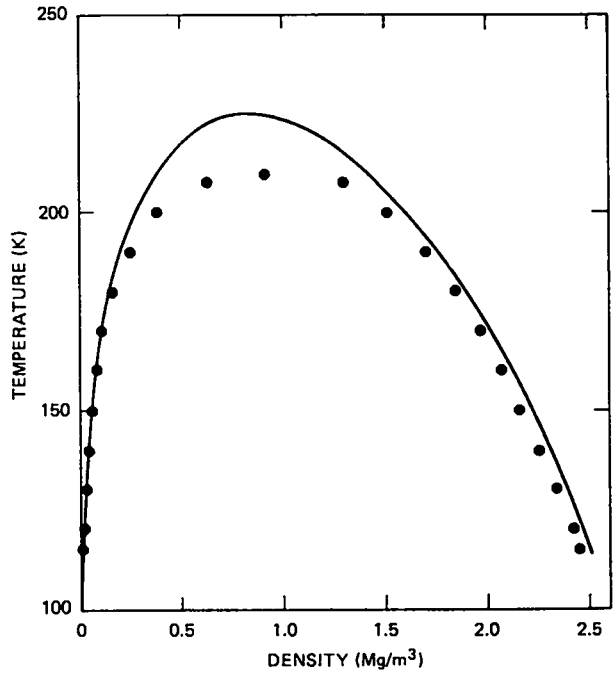

Fig. 15.
Temperature and density on the coexistence curve for krypton. Symbols are the same as in Fig. 13.

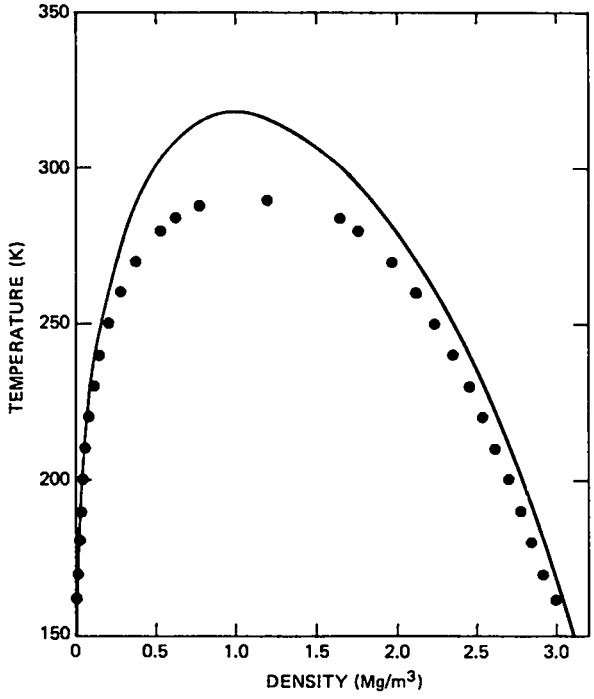

Fig. 16.
Temperature and density on the coexistence curve for xenon. Symbols are the same as in Fig. 13.

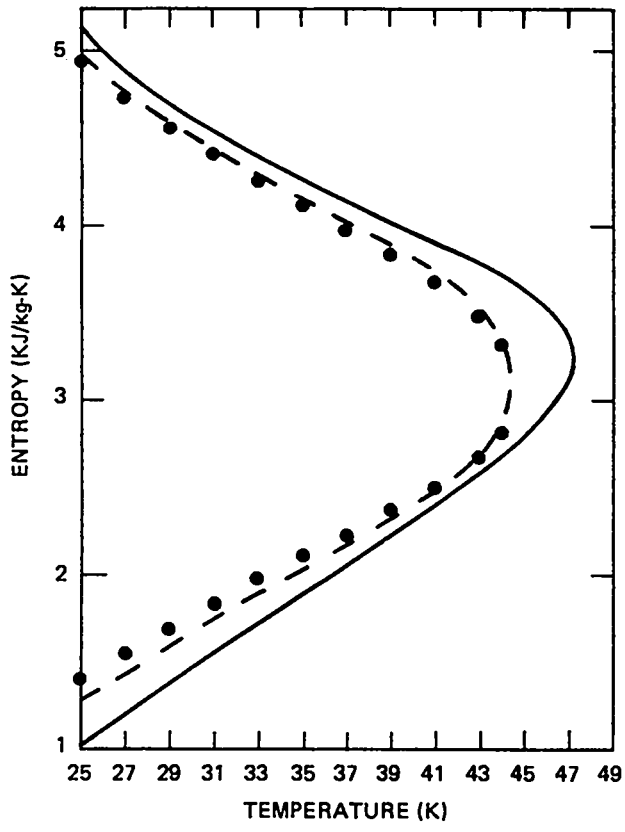

Fig. 17.
Entropy on the coexistence curve for neon. The solid line is calculated using the theoretical densities for the saturated vapor and liquid phase. The dashed line is calculated using the experimental densities. Experimental data are from Ref. 27.

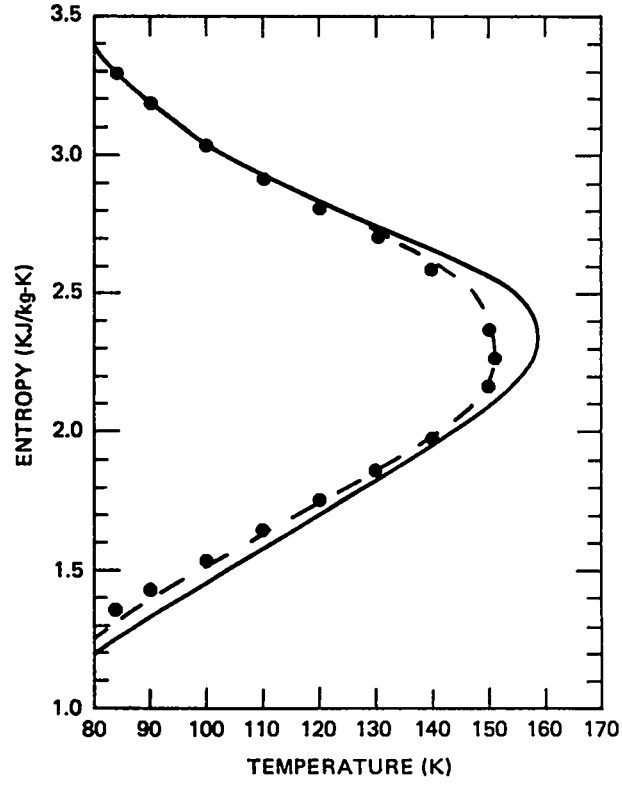

Fig. 18.
Entropy on the coexistence curve for argon. Symbols are the same as in Fig. 17.

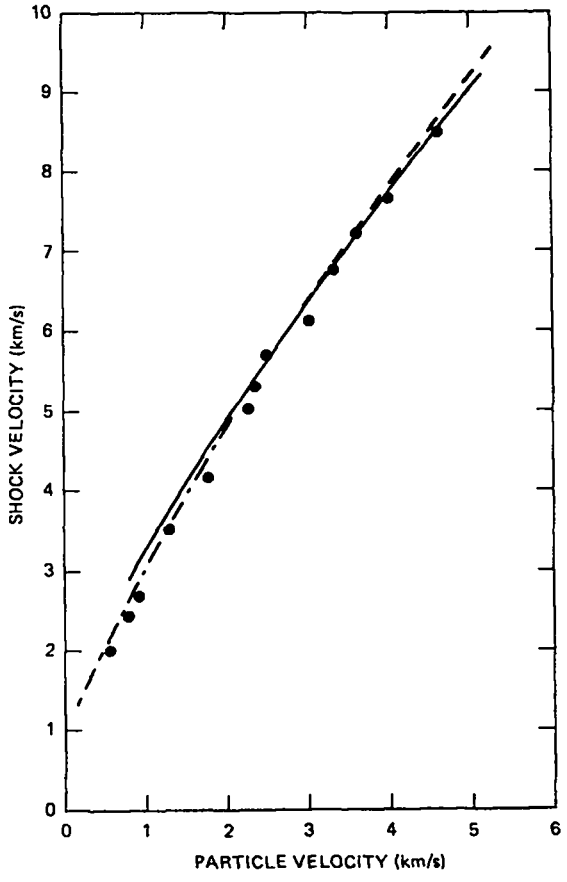

Fig. 19.
Hugoniot for solid argon at an initial density of 1.65 Mg/m^3 and an initial temperature of 75 K. Circles are experimental data from Ref. 30. The solid line is our calculation for the liquid, including corrections for electronic excitation. The dashed line is a calculation in which the electronic terms are omitted. The dashed-dotted line is a calculation for the shocked solid.

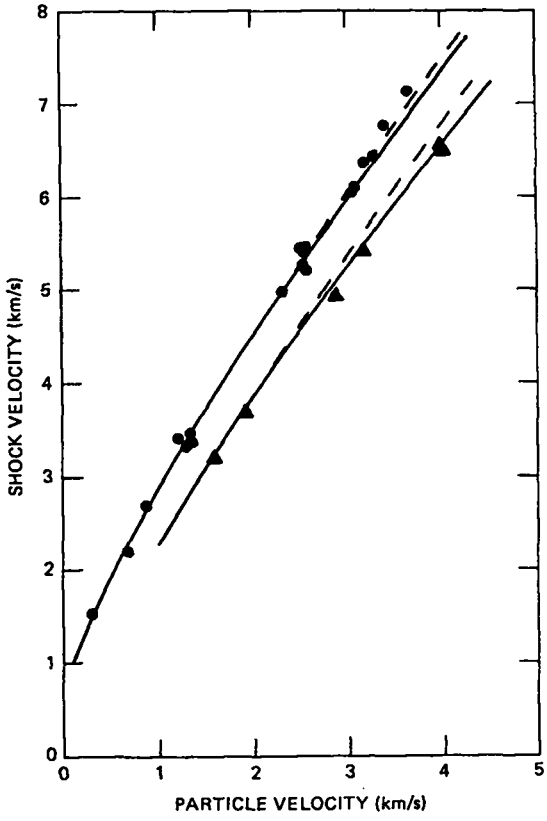

Fig. 20.
Hugoniots for liquid argon. Circles correspond to an initial density of 1.4 Mg/m^3 and an initial temperature of 86 K and triangles correspond to an initial density of 0.919 Mg/m^3 and an initial temperature of 148 K. Experimental data are from Ref. 30. Calculations shown by the solid line include electronic excitation; those shown by a dashed line do not.

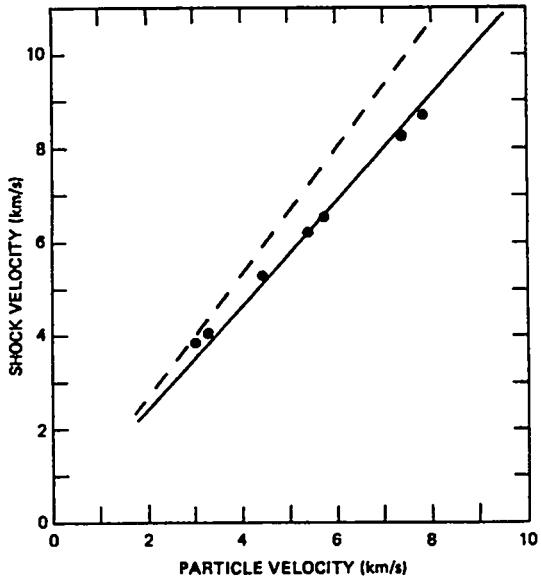

Fig. 21.
Hugoniot for argon at an initial density of 0.0013 Mg/m^3 and an initial temperature of 300 K. Experimental data are from Ref. 32. Calculations shown by the solid line include electronic excitation; those shown by a dashed line do not.

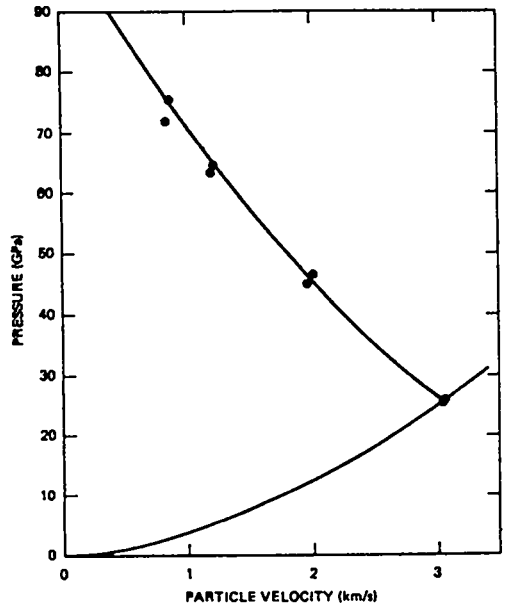

Fig. 22.
Reflected shock data for liquid argon. The initial density and temperature were 1.4 Mg/m^3 and 86 K; the density, pressure, and particle velocity of the singly shocked state were 2.86 Mg/m^3, 25.7 Gpa, and 3.06 km/sec. Experimental data are from Ref. 33. Calculated results are shown by the solid lines.

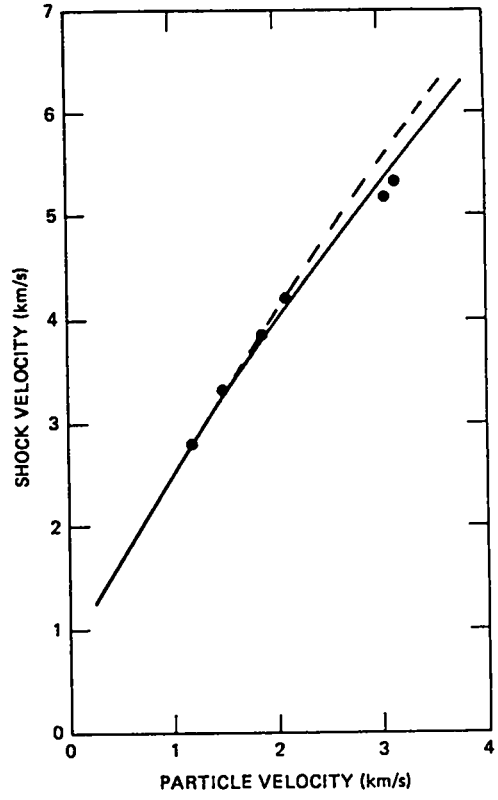

Fig. 23.
Hugoniot for liquid xenon at an initial density of 3.095 Mg/m^3 and an initial temperature of 165 K. Circles are experimental data from Ref. 34. Calculations shown by a solid line include electronic excitation; those shown by a dashed line do not.

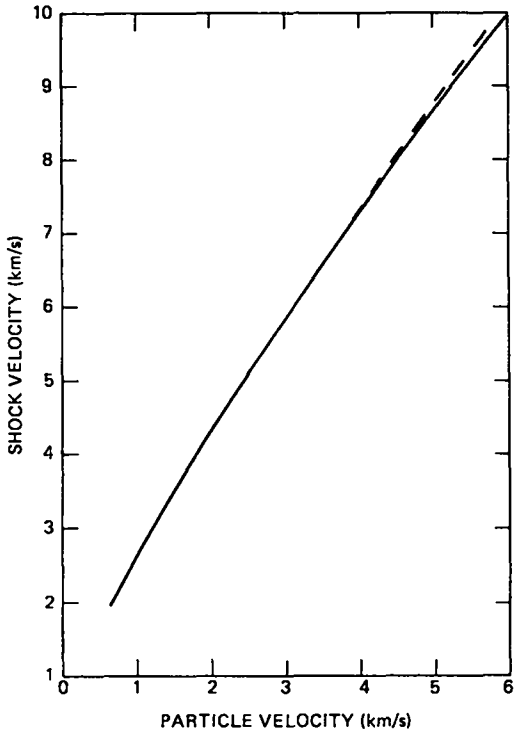

Fig. 24.
Predicted Hugoniot for liquid neon at an initial density of 1.248 Mg/m^3 and an initial temperature of 24.5 K. Calculations shown by a solid line include electronic excitation; those shown by a dashed line do not.

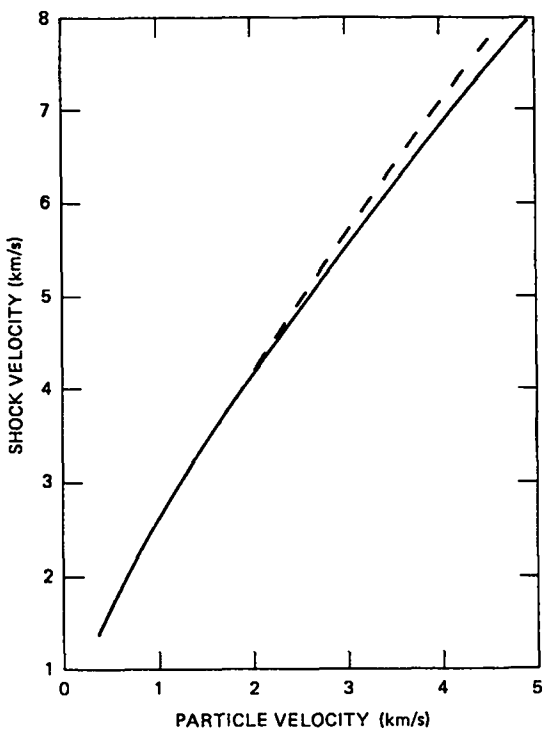

Fig. 25.
Predicted Hugoniot for liquid krypton at an initial density of 2.45 Mg/m^3 and an initial temperature of 115.8 K. Calculations shown by a solid line include electronic excitation; those shown by a dashed line do not.

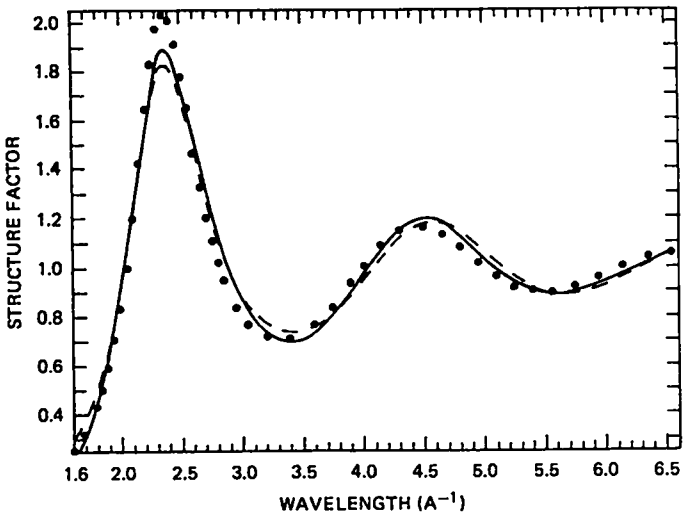

Fig. 26.
Structure factor for liquid neon at a density of 1.119 Mg/m^3 and temperature of 35.05 K. Circles are neutron-diffraction data from Ref. 38. The dashed line is the calculated structure factor of the hard-sphere reference system. The solid line includes corrections for the soft core.

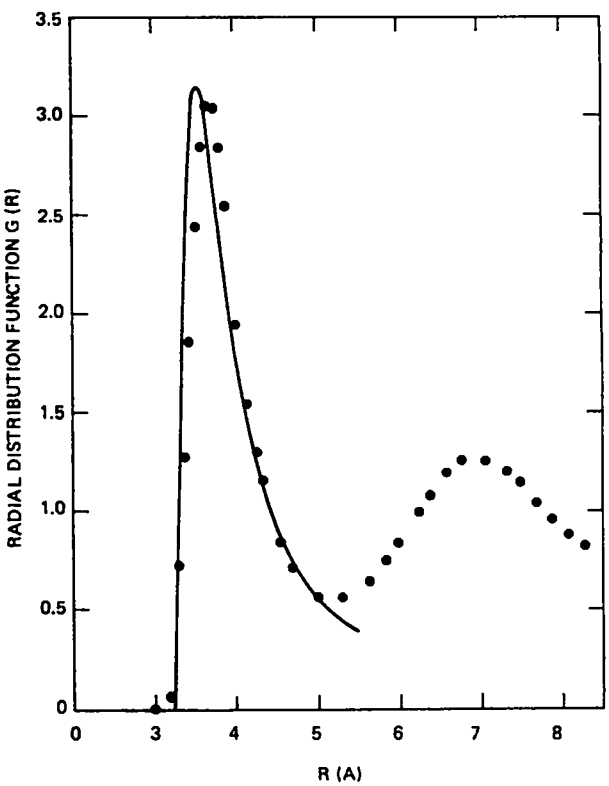

Fig. 27.
Radial distribution function for liquid argon at a density of 1.409 Mg/m^3 and a temperature of 85 K. Circles are neutron-scattering data from Ref. 39. The solid line is our calculation for the first peak.

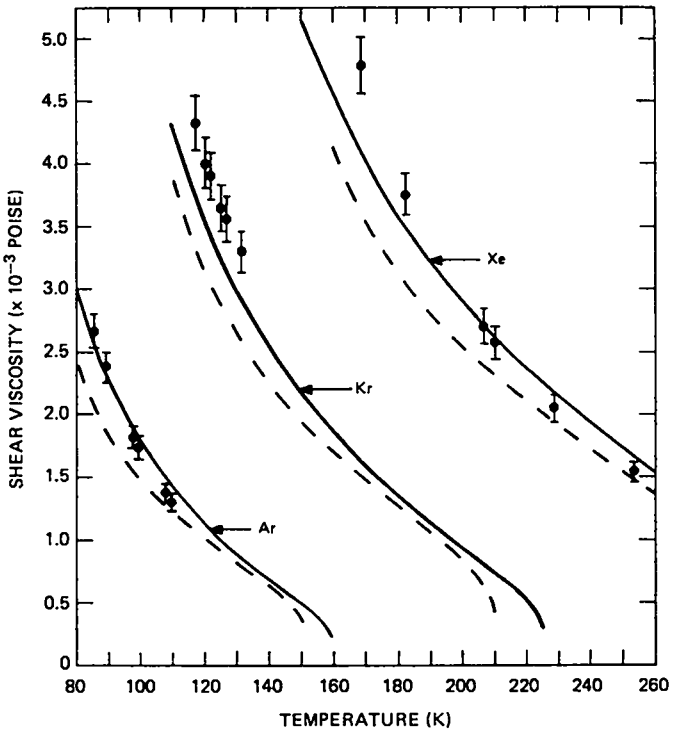

Fig. 28.
Shear viscosities for liquid argon, krypton, and xenon. Experimental data are from Ref. 45. Calculations shown by solid lines use the theoretical liquid densities on the coexistence curve. Calculations shown by dashed lines use the experimental densities.

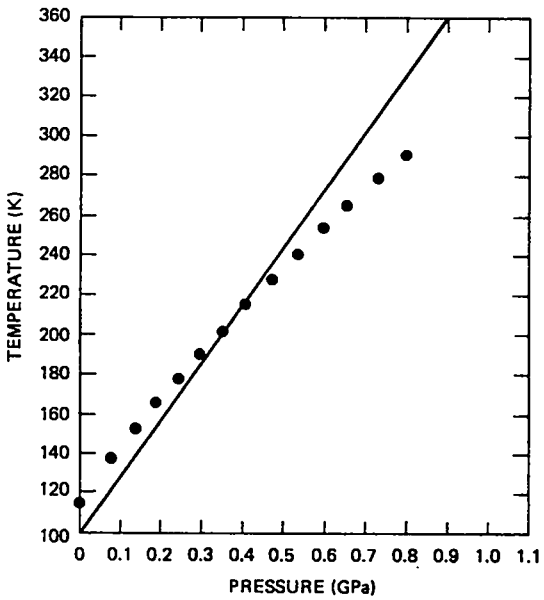

Fig. 29.
Melting curve for krypton. Circles are experimental data from Ref. 46. The solid line was calculated using the CRIS model for the liquid phase and the Debye model for the solid phase.

ACKNOWLEDGMENT

We thank J. D. Johnson for providing the TFD tables used in the Hugoniot calculations.

APPENDIX A

TFD THEORY AND THE COLD CURVE AT HIGH DENSITIES

The TFD statistical model of the atom is used often as an interpolation formula in calculations of EOS at high densities.[47,48] The TFD theory is found to agree fairly well with band-theoretical calculations at pressures of about 1 TPa (10 Mbar) and above.[49] However, good results can be obtained at much lower pressures by making simple empirical corrections to the TFD results.

Here we describe a high-density interpolation formula, based upon TFD theory, that has given good results when applied to many materials. This formula is joined smoothly at an arbitrary density to the cold curve at lower pressures. In this report, we matched the TFD expression to the exp-6 formula, which was fitted to experimental data at low densities. Except for the Hugoniots, our calculated results are insensitive to the density used in the TFD match.

We use the following expressions for the internal energy E_C and pressure P_C on the cold curve at high densities.

$$E_C(\rho) = [E_T(\rho) - \Delta E_T]y(\rho) + \Delta E_C \qquad \text{(A-1)}$$

and

$$P_C(\rho) = P_T(\rho)y(\rho) + \rho^2[E_T(\rho) - \Delta E_T]dy/d\rho \quad , \qquad \text{(A-2)}$$

where

$$y(\rho) = 1 + b_1/\rho + b_2/\rho^{4/3} + b_3/\rho^{5/3} \qquad \text{(A-3)}$$

and $E_T(\rho)$ and $P_T(\rho)$ are the internal energy and pressure predicted by TFD theory. To join this expression to the cold curve at some density ρ_M, we require that

$$\Delta E_T = E_T(\rho_M) \tag{A-4}$$

and

$$\Delta E_C = E_C(\rho_M) \quad . \tag{A-5}$$

We calculated the coefficients b_1, b_2, and b_3 by requiring that the pressure and its first two derivatives be continuous at ρ_M.

The TFD results are approximated by the following analytic expressions.

$$E_T(\rho) = \frac{1505.2125\ Z}{WX^5}\ e^{-F(X)} \quad , \tag{A-6}$$

$$P_T(\rho) = \frac{1003.475}{X^5}\ e^{-F(X)}\left(1 + \tfrac{1}{2} \times \frac{dF}{dX}\right) \quad , \tag{A-7}$$

$$X = (W/Z\rho)^{1/3} \quad , \tag{A-8}$$

and

$$F(X) = C_1X + C_2X^2 + C_3\ X^2\ \ln X \quad . \tag{A-9}$$

Here Z is the atomic number and W is the atomic weight. The quantities C_1, C_2, and C_3 are given by

$$C_1 = 0.703473 + 1.130622\ Z^{2/3} \tag{A-10}$$

$$C_2 = 0.3 - 0.00245\ Z^{5/2}/(1 + 0.0028Z^2) \quad , \tag{A-11}$$

and

$$C_3 = 0.6 + 0.0386\ Z^{4/3} \quad . \tag{A-12}$$

These formulas, which we obtained by fitting Cowan's[50] numerical TFD results, are better than 2% accurate at pressures above 100 GPa; at lower pressures, they

give results that are sufficiently accurate for the interpolation procedure described above.

The parameters used in our high-density formula for the rare gases are given in Table A-I.

TABLE A-I

PARAMETERS IN THE STATISTICAL ATOM FORMULA

FOR THE COLD CURVE AT HIGH DENSITIES

Parameter	Neon	Argon	Krypton	Xenon
Z	10.	18.	36.	54.
W	20.179	39.948	83.8	131.3
b_1	-12.0592	36.3218	41.5063	87.8497
b_2	19.7611	-99.4454	-140.004	-283.796
b_3	-8.52989	66.2120	112.820	227.856
ΔE_T	7.72287	1.43103	0.969247	0.342025
ΔE_C	6.32801	0.466884	0.302734	0.211483
C_1	5.95131	8.46886	13.0303	16.8562
C_2	-0.305280	-1.46584	-3.81580	-5.42832
C_3	1.43161	2.42089	5.18836	8.47854

APPENDIX B

TFD THEORY AND THERMAL ELECTRONIC CONTRIBUTIONS TO THE THERMODYNAMIC PROPERTIES

For most of the calculations described in this report, we can assume that the atoms are in the ground electronic state. In the shock-wave experiments however, there is sufficient thermal energy to cause significant excitation, so corrections must be added to the thermodynamic properties. In this work, the corrections are computed from the temperature-dependent TFD theory.[29]

We use two computer codes used for TFD calculations at the Los Alamos Scientific Laboratory. One code, written by R. D. Cowan, uses the nonlocal exchange formulation of Cowan and Ashkin.[29,50] The other code, CANDIDE, written by D. A. Liberman,[51] uses a local exchange approximation. For the purposes of this report, both codes give essentially the same results. CANDIDE was used for xenon, and Cowan's code was used for neon, argon, and krypton.

TFD theory computes the electronic contributions to the thermodynamic functions of an atom; the atoms are assumed to be stationary, and there is no contribution from zero-point and thermal motion of the nuclei. Because of the semiclassical nature of the statistical theory, the discrete atomic energy levels are smeared out. At zero temperature the theory gives poor results, except at high densities. It does not predict solid binding, or give any dependence of the thermodynamic properties on the configuration of the nuclei. However, the thermal contributions predicted by TFD theory are fairly realistic, particularly for temperatures in excess of 10^4 K.[51] At lower temperatures the thermal electronic terms are small relative to the nuclear contributions, so errors in the TFD theory are not too serious.

In this work, the TFD terms were computed from tables prepared by J. D. Johnson. The zero-temperature isotherms were subtracted, leaving only the finite temperature contributions. Next, the tables were scaled by dividing by the results for a noninteracting electron gas. The reduced tables were input to the PANDA code, which computes the TFD terms by interpolation and adds them to the results of the liquid model.

The low density Hugoniot for argon shown in Fig. 21 provides a significant test of the TFD theory because of the high degree of electronic excitation. The fact that the model agrees quite well with the data shows that TFD theory is a reasonable model for calculating the effects of electronic excitation.

REFERENCES

1. M. L. Klein and J. A. Venables, Rare Gas Solids (Academic Press, New York, 1976).

2. J. A. Barker and D. Henderson, "What is 'Liquid'? Understanding the States of Matter," Rev. Mod. Phys. 48, 587 (1976).

3. J. A. Barker, D. Henderson, and W. R. Smith, "Pair and Triplet Interactions in Argon," Mol. Phys. 17, 579 (1969).

4. G. I. Kerley, "A New Model of Fluids," Los Alamos Scientific Laboratory report LA-4760 (December 1971).

5. G. I. Kerley, "Perturbation Theory and the Thermodynamic Properties of Fluids," submitted to J. Chem. Phys.

6. J. P. Hansen and I. R. MacDonald, Theory of Simple Liquids (Academic Press, London, 1976) pp. 145-150.

7. H. C. Andersen, D. Chandler, and J. D. Weeks, "Roles of Repulsive and Attractive Forces in Liquids: The Equilibrium Theory of Classical Fluids," Adv. Chem. Phys. 34, 105 (1976).

8. S. B. Trickey and F. R. Green, Jr., "One-Electron Theory of the Bulk Properties of Crystalline Ar, Kr, and Xe," Phys. Rev. B8, 4822 (1973).

9. J. O. Hirschfelder, C. F. Curtiss, and R. B. Bird, Molecular Theory of Gases and Liquids (John Wiley & Sons, New York, 1954) pp. 180-181.

10. I. Ebbsjö, "Thermodynamical Properties of the Solidified Rare Gases," A B Atomenergi report AE-442, Studsvik, Sweden, (1971).

11. V. Zharkov and V. Kalinin, Equation of State for Solids at High Pressures and Temperatures (Consultants Bureau, New York, 1971) pp. 241-2.

12. G. L. Pollack, "The Solid State of Rare Gases," Rev. Mod. Phys. 36, 748 (1964).

13. R. Hultgren, P. D. Desai, D. T. Hawkins, M. Gleiser, K. K. Kelley, and D. D. Wagman, Selected Values of the Thermodynamic Properties of the Elements, (American Society for Metals, Metals Park, Ohio, 1972).

14. M. V. Bobetic and J. A. Barker, "Lattice Dynamics with Three-Body Forces: Argon," Phys. Rev. B2, 4169 (1970).

15. M. S. Anderson, R. Q. Fugate, and C. A. Swenson, "Equation of State for Solid Neon to 20 kbar," J. Low. Temp. Phys. 10, 345 (1973).

16. M. S. Anderson and C. A. Swenson, "Experimental Equations of State for the Rare Gas Solids," J. Phys. Chem. Solids 36, 145 (1975).

17. C. G. Homan, J. Frankel, D. P. Kendall, J. A. Barrett, and T. E. Davidson, "Acoustic Velocity Ratios in Solid Argon at 75K up to Static Pressures of 150 kbar," in 6th AIRAPT Conference on High Pressure Science and Technology, Boulder, Colo., (1977), K. D. Timmerhaus and M. Barber, Eds. (Plenum Press, New York, 1979).

18. K. Syassen and W. B. Holzapfel, "High-Pressure Equation of State for Solid Xenon," Phys. Rev. B18, 5826 (1978).

19. R. M. Gibbons, "The Equation of State of Neon Between 27 and 70K," Cryogenics 9, 251 (1969).

20. D. Vidal, L. Guengant et M. Lallemand, "Vitesse des Ultrasons dans les Gaz Rares Sous Haute Pression a la Temperature de 298.15 K," Physica (Utrecht) 96A, 545, (1979).

21. W. B. Street and L. A. K. Staveley, "Experimental Study of the Equation of State of Liquid Argon," J. Chem. Phys. 50, 2302 (1969).

22. R. K. Crawford and W. B. Daniels, "Equation of State Measurements in Compressed Argon," J. Chem. Phys. 50, 3171 (1969).

23. S. L. Robertson, S. E. Babb, Jr., and G. J. Scott, "Isotherms of Argon to 10000 bars and 400° C," J. Chem. Phys. 50, 2160 (1969).

24. D. H. Liebenberg, R. L. Mills, and J. C. Bronson, "High Pressure Apparatus for Simultaneous Adiabatic and Isothermal Compressibility Measurements: Data on Argon to 13 kbar," J. Appl. Phys. 45, 741 (1974).

25. W. B. Street and L. A. K. Staveley, "Experimental Study of the Equation of State of Liquid Krypton," J. Chem. Phys. 55, 2495 (1971).

26. W. B. Street, L. S. Sagan, and L. A. K. Staveley, "An Experimental Study of the Equation of State of Liquid Xenon," J. Chem. Thermodynamics 5, 633 (1973).

27. N. B. Vargaftik, Tables on the Thermophysical Properties of Liquids and Gases (John Wiley & Sons, New York, 1975) 2nd Ed.

28. B. P. Singh and S. K. Sinha, "Quantum Corrections to the Equilibrium Properties of Dense Fluids: Application to Hard-Sphere Fluids," J. Chem. Phys. 67, 3645 (1977).

29. R. D. Cowan and J. Ashkin, "Extension of the Thomas-Fermi-Dirac Statistical Theory of the Atom to Finite Temperatures," Phys. Rev. 105, 144 (1957).

30. R. D. Dick, R. H. Warnes, and J. Skalyo, Jr., "Shock Compression of Solid Argon," J. Chem. Phys. 53, 1648 (1970).

31. M. van Thiel and B. Alder, "Shock Compression of Argon," J. Chem. Phys. 44, 1056 (1966).

32. R. H. Christian and F. L. Yarger, "Equation of State of Gases by Shock Wave Measurements. I. Experimental Method and the Hugoniot of Argon," J. Chem. Phys. 23, 2042 (1955).

33. W. L. Seitz and J. Wackerle, "Reflected Shock Hugoniot for Liquid Argon Between 0.26 and 0.74 Megabars," Bull. Am. Phys. Soc. 17, 1093 (1972); LASL Shock Hugoniot Data, S. P. Marsh, Ed. (University of California Press, Berkeley) in press.

34. "Compendium of Shock Wave Data", M. van Thiel, Ed., Lawrence Livermore Laboratory report UCRL-50108, Rev. 1 (June 1977).

35. R. N. Keeler, M. van Thiel, and B. J. Alder, "Corresponding States at Small Interatomic Distances," Physica (Utrecht) 31, 1437 (1965).

36. D. A. Nelson, Jr., and A. L. Ruoff, "Metallic Xenon at Static Pressures," Phys. Rev. Lett. 42, 383 (1969).

37. L. Verlet and J.-J. Weis, "Equilibrium Theory of Simple Liquids," Phys. Rev. A5, 939 (1972).

38. L. A. de Graaf and B. Mozer, "Structure Study of Liquid Neon by Neutron Diffraction," J. Chem. Phys. 55, 4967 (1971).

39. J. L. Yarnell, M. J. Katz, R. G. Wenzel, and S. H. Koenig, "Structure Factor and Radial Distribution Function for Liquid Argon at 85 K," Phys. Rev. A7, 2130 (1973).

40. B. E. Kirsten and C. J. Pings, "Structure Determination of Liquid Argon by X-ray Diffraction," J. Chem. Phys. 66, 5730 (1977).

41. J. H. Dymond and B. J. Alder, "Van der Waals Theory of Transport in Dense Fluids," J. Chem. Phys. 45, 2061 (1966).

42. H. L. Frisch and B. Berne, "High-Temperature Expansion of Thermal Transport Coefficients," J. Chem. Phys. 43, 250 (1965).

43. J. H. Dymond, "Corrected Enskog Theory and the Transport Coefficients of Liquids," J. Chem. Phys. 60, 969 (1974).

44. B. J. Alder, D. M. Gass, and T. E. Wainwright, "Studies in Molecular Dynamics. VIII. The Transport Coefficients for a Hard-Sphere Fluid," J. Chem. Phys. 53, 3813 (1970).

45. B. Y. Baharudin, D. A. Jackson, and P. E. Schoen, "Bulk Viscosity of Liquid Argon, Krypton, and Xenon," Phys. Lett. 51A, 409 (1975).

46. R. K. Crawford and W. B. Daniels, "Experimental Determination of the P-T Melting Curves of Kr, Ne, and He," J. Chem. Phys. 55, 5651 (1971).

47. J. F. Barnes, "Statistical Atom Theory and the Equation of State of Solids," Phys. Rev. 153, 269 (1967).

48. S. L. Thompson and H. S. Lauson, "Improvements in the Chart-D Radiation-Hydrodynamic Code III: Revised Analytic Equations of State," Sandia Laboratories report SC-RR-71074 (March 1972).

49. D. A. Liberman, "Self-Consistent Field Calculations of Bulk Properties of Solids," in Les Proprietes Physiques des Solides sous Pression, Colloq. Int. Cent. Nat. Rech. Sci., No. 188, Grenoble, 1969, pp. 35-41, Ed. du CNRS, Paris (1970).

50. R. D. Cowan, Los Alamos Scientific Laboratory, unpublished data, 1958.

51. D. A. Liberman and B. I. Bennett, Los Alamos Scientific Laboratory, unpublished data, 1979.

Printed in the United States of America. Available from
National Technical Information Service
US Department of Commerce
5285 Port Royal Road
Springfield, VA 22161

Microfiche $3.00

001-025	4.00	126-150	7.25	251-275	10.75	376-400	13.00	501-525	15.25
026-050	4.50	151-175	8.00	276-300	11.00	401-425	13.25	526-550	15.50
051-075	5.25	176-200	9.00	301-325	11.75	426-450	14.00	551-575	16.25
076-100	6.00	201-225	9.25	326-350	12.00	451-475	14.50	576-600	16.50
101-125	6.50	226-250	9.50	351-375	12.50	476-500	15.00	601-up	

Note: Add $2.50 for each additional 100-page increment from 601 pages up.